ACS Photonics

pubs.acs.org/journal/apchd5

Article

Anti-Stokes Light Scattering Mediated by Electron Transfer Across a Biased Plasmonic Nanojunction

Shuyi Liu, Adnan Hammud, Martin Wolf, and Takashi Kumagai*

Cite This: *ACS Photonics* 2021, 8, 2610–2617

Read Online

ACCESS | Metrics & More | Article Recommendations | Supporting Information

ABSTRACT: Light scattering from plasmonic nanojunctions is routinely used to assess their optical properties. However, the microscopic mechanism remains imperfectly understood, and an accurate description requires the experiment in a well-defined environment with a highly precise control of the nanojunction. Here we report on inelastic light scattering (ILS) from plasmonic scanning tunneling microscope (STM) junctions under ultrahigh vacuum and cryogenic conditions. We particularly focus on anti-Stokes continuum generation in the ILS spectra with a narrowband continuous-wave laser excitation, which appears when an electrical bias is applied between the tip and the surface. This anti-Stokes continuum is commonly observed for various STM junctions at ∼10 K, corroborating that it is a universal phenomenon in electrically biased plasmonic nanojunctions. We propose that the microscopic mechanism underlying the anti-Stokes continuum generation is explained by ILS accompanied by electron transfer across the STM junction, whereby the excess energy is provided by the applied bias voltage. This process occurs through either photoluminescence (PL) or electronic Raman scattering (ERS). By recording the ILS spectra in parallel with STM-induced luminescence, we show that ERS becomes dominant when the excitation wavelength matches the plasmonic resonance of the STM junction, whereas PL mainly contributes to the off-resonance excitation. Our results provide an in-depth understanding of ILS by plasmonic nanojunctions and demonstrate that the anti-Stokes continuum can arise from a nonthermal mechanism.

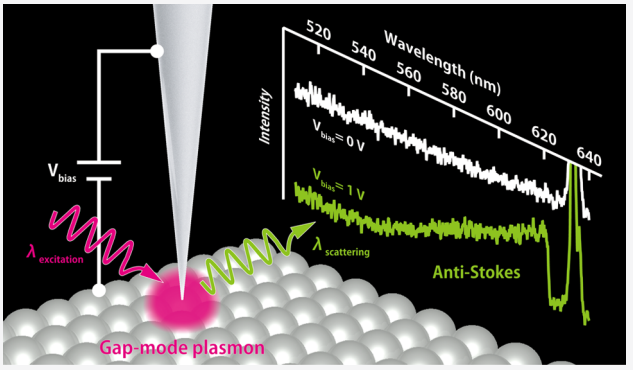

KEYWORDS: *plasmonic nanojunction, electronic Raman scattering, photoluminescence, scanning tunneling microscopy*

Light scattering from metal nanostructures is of fundamental importance in plasmonics and nanooptics since it gives basic information regarding their optical properties.[1] However, the underlying microscopic mechanism has been intensely debated over the last two decades.[2−20] These studies showed that the inelastic light scattering (ILS) spectra are strongly dependent on the plasmonic properties determined by the nanoscale morphology of metals as well as the excitation wavelength. The ILS spectra commonly exhibit a broad continuum in the visible and near-infrared range.[2−20] A similar continuum has also been recognized as a spectral background in surface- and tip-enhanced Raman spectroscopy,[21−24] which interferes with narrow vibrational peaks.[25−29] The spectral continuum arises from ILS by conduction electrons in a metal, namely, via photoluminescence (PL) or electronic Raman scattering (ERS). PL and ERS are an incoherent and coherent light scattering process, respectively.[30] PL originates from a real electronic excitation of the system that is followed by radiative recombination of excited electron−hole pairs,[31,32] whereas ERS occurs instantaneously via virtual states.[15,33,34] In a density matrix, PL and ERS involve transitions via diagonal and off-diagonal elements, respectively.[30] Although PL and ERS in metals are rather inefficient, these processes can be largely enhanced in plasmonic nanostructures,[35−38] whereby, in addition to the field-enhancement effect, the strong confinement of the plasmonic field will play a crucial role as it results in a large momentum uncertainty and a field gradient, promoting intraband transitions (requiring a change in the momentum) and higher-order multipolar transitions.[37,39,40] However, it is not straightforward to distinguish PL and ERS in the ILS spectra of plasmonic nanostructures, because both processes exhibit a similar spectral feature (i.e., broad continuum).

Another controversial observation of ILS by plasmonic nanostructures is anti-Stokes continuum generation where the incident photons gain an excess energy during the scattering process through the ERS[12,15,19,44] or PL[10,14,20] mechanism. Although this anti-Stokes continuum is applicable for nano-

Received: March 16, 2021
Published: August 12, 2021

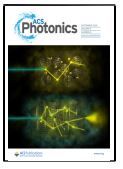

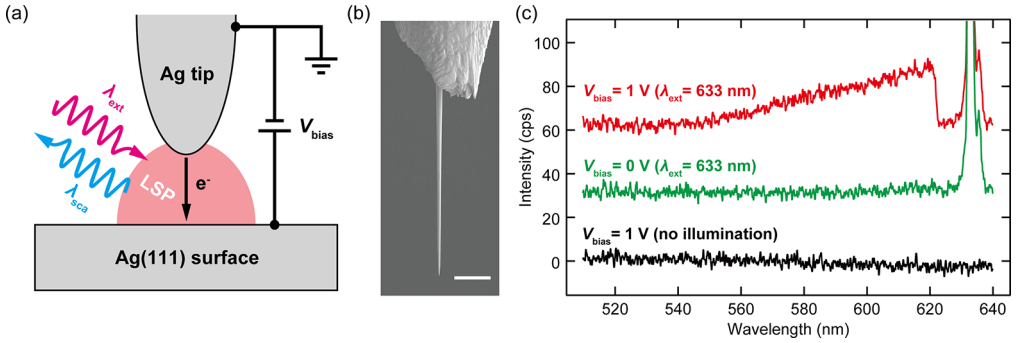

Figure 1. (a) Schematic of the experiment. (b) Scanning electron micrograph of an FIB-Ag tip. The scale bar is 10 μm. (c) ILS spectra (anti-Stokes regime) measured for the Ag tip−vacuum−Ag(111) junction (λ_{ext} = 633 nm, P_{ext} = 0.37 mW μm^{-2}, 10 K). The red and green curves are recorded at V_{bias} = 1 V and −1.8 mV, respectively, while keeping the tip−surface distance identical at an STM set-point of V_{bias} = 1 V and j_t = 80 nA. The black curve shows an STL spectrum recorded without illumination at V_{bias} = 1 V and j_t = 80 nA. The scattering spectra are vertically shifted for clarity.

imaging[41] and nanothermometry,[42−44] a proper interpretation requires accurate knowledge of the microscopic light-scattering mechanism. The anti-Stokes continuum generation was investigated for plasmonic nanoparticles,[10,12,14,15,19,20,44] but it remains unexplored for plasmonic nanocavities important for many applications in ultrasensitive optical spectroscopies and enhanced photophysical/chemical processes, benefiting from extreme enhancement and confinement of plasmonic fields. In nanocavities, an electrical potential between separated nanostructures can be used as an additional tuning parameter of the plasmonic properties.[45] Such electrically biased plasmonic nanojunctions are of particular interest in nanoscale optoelectronic devices[46−48] and in optical nanoscopy combined with scanning tunneling microscopy (STM).[49,50] Optical properties of plasmonic STM junctions have been extensively investigated using scanning tunneling luminescence (STL) spectroscopy,[51,52] and advanced low-temperature tip-enhanced spectroscopy recently demonstrated the unprecedented sensitivity and spatial resolution that enable spectral mapping at the submolecular scale.[53−55] However, the broad continuum generation in the ILS spectra has not been focused so far in the STM junctions.

Here we report on the anti-Stokes continuum generation in ILS from plasmonic STM junctions under ultrahigh vacuum (UHV) and cryogenic conditions. The anti-Stokes continuum is observed when the junction is electrically biased. Various junctions consisting of a sharp Ag tip and different single-crystal surfaces, including Ag tip−vacuum−Ag(111), Ag tip−vacuum−Ag(100), Au tip−vacuum−Au(111), and Ag tip−single C_{60} molecule−vacuum−Ag(111) junctions, are examined in order to show that the bias-induced anti-Stokes continuum generation is a universal phenomenon. The complex ILS mechanism is scrutinized by recording STL and ILS spectra in parallel and comparing their spectral intensity. We propose a physical model that the ILS is mediated by electron transfer across the biased junction, and the relative contribution from the PL and ERS mechanisms is determined by spectral matching between the plasmonic resonance of the junction and the excitation wavelength.

METHODS

Sample Preparation. All experiments were performed in UHV chambers (base pressure: <5 × 10^{-10} mbar). The Ag(111), Ag(100), and Au(111) surfaces were purchased from MaTeck GmbH and were cleaned under UHV conditions by repeated cycles of Ar^+ sputtering and annealing up to 670, 600, and 700 K, respectively. The atomically clean surface was confirmed by the STM measurement. C_{60} was purchased from SigmaAldrich and used without further purification. The molecules were evaporated at 600 K from a K-cell evaporator onto the Ag(111) surface held at room temperature.

STM Measurement. We used a low-temperature STM from UNISOKU Ltd. (modified USM-1400) operated with Nanonis SPM Controller (SPECS GmbH). The bias voltage (V_{bias}) was applied to the sample, and the tip was grounded. The tunneling current (j_t) was collected from the tip. The Ag tips were first chemically etched from an Ag wire and then further sharpened by focused ion beam milling to yield a highly reproducible plasmonic response (see Figure 1b and ref 56 for more details).

Light Scattering Spectroscopy. The incident laser beam was sent into the UHV chamber equipped with the low-temperature STM unit through a fused silica window. The excitation laser was focused to the STM junction with an *in situ* Ag-coated parabolic mirror (numerical aperture of ∼0.6) mounted on the cold STM stage. The parabolic mirror was precisely aligned using piezo motors (Attocube GmbH) enabling three translational and two rotational motions. For excitation we used a solid-state lasers for 532 nm and a HeNe laser for 633 nm. A bandpass filter was used for the HeNe laser. The incident beam was linearly polarized along the tip axis (p-polarization). The scattered light was collected by the same parabolic mirror and was detected outside of the UHV chamber with a grating spectrometer (AndorShamrock 303i) equipped with the back illuminated CCD camera (Newton 970). The scattered light was separated by a beamsplitter and filtered by a notch filter (NF533-17 and NF633-25 from Thorlabs) before coupling to the spectrometer via an optical fiber.

RESULTS AND DISCUSSIONS

Figure 1a illustrates the experiment. An Ag tip−vacuum−Ag(111) junction at 10 K is irradiated by a focused narrowband cw laser, which leads to strong field enhancement when the incident wavelength matches the localized surface plasmon resonance (LSPR) of the junction. The tip is positioned over an atomically flat terrace of the Ag(111) surface. Figure 1c shows the anti-Stokes regime of the ILS spectra obtained for an excitation wavelength (λ_{ext}) of 633 nm. The anti-Stokes continuum appears when the electrical bias

https://doi.org/10.1021/acsphotonics.1c00402
ACS Photonics 2021, 8, 2610−2617

(V_{bias} = 1 V) is applied to the junction, whereas no signal is observed at V_{bias} = 0 V. For both cases, the tip−surface distance is kept constant so that the field enhancement in the junction remains identical. A possible contribution from electroluminescence through multiple inelastic scattering of tunneling electrons[57,58] can be excluded because the anti-Stokes continuum is absent at V_{bias} = 1 V without irradiation. Also, two-photon-induced PL[35−37] can be excluded because the intensity of the anti-Stokes continuum depends linearly on the incident laser power density, P_{ext} (Supporting Information, Figure S1). Therefore, the anti-Stokes continuum must originate from the scattering process associated with the V_{bias}.

Figure 2 shows the V_{bias}-dependence of the ILS spectra recorded for an Ag tip−vacuum−Ag(111) junction. The

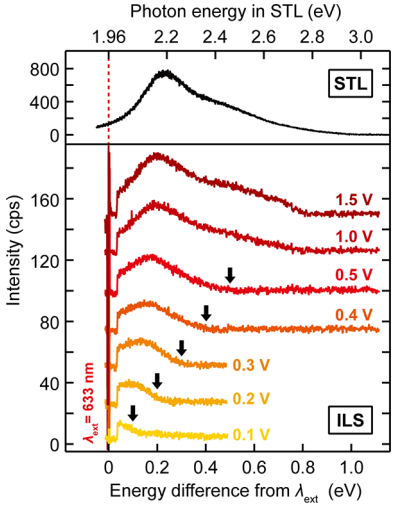

Figure 2. (Top) STL spectrum (V_{bias} = 3 V, j_t = 8 nA, 10 K). (Bottom) ILS spectra (anti-Stokes branch) recorded at different bias voltages and the same current of 80 nA (λ_{ext} = 633 nm, P_{ext} = 0.37 mW μm^{-2}, 10 K). The spectra are vertically shifted for clarity (except for V_{bias} = 0.1 V). The horizontal axis at the bottom is the energy difference relative to the excitation photon energy of 1.96 eV. The arrows indicate the maximum energy that can be supplied by V_{bias}. The sharp cutoff near 0 eV is caused by the notch filter, which also suppresses the background intensity.

horizontal axis in the bottom panel represents the energy gain of the scattered photons with respect to the incident wavelength (λ_{ext} = 633 nm, $\hbar\nu$ = 1.96 eV). The top panel displays the STL spectrum obtained at V_{bias} = 3 V, where the LSPR of the junction (gap-mode plasmon) is observed. The arrows in Figure 2 indicate the maximum energy that can be supplied by V_{bias}. It is clear that the cutoff energy of the anti-Stokes continuum correlates with V_{bias} at lower bias (<0.5 V). However, the spectral shape resembles the STL at higher voltages (V_{bias} = 1 and 1.5 V), indicating the contribution of the gap-mode plasmon. Note that a slight shift of the resonance position between the STL and ILS spectra is caused by a different tip−surface distance (~2 Å displacement) as they are recorded at a different STM set-point. Similar results were obtained for the opposite bias (Supporting Information, Figure S2) and also with a different excitation wavelength (Supporting Information, Figure S3).

In order to verify that the V_{bias}-induced anti-Stokes continuum is a universal phenomenon, we examine different junctions, namely Ag tip−vacuum−Ag(100), Au tip−vacuum−Au(111), and Ag tip−C_{60} molecule−vacuum−Ag(111) junctions (Figure 3). A single C_{60} molecule was attached to the tip apex by picking up from the surface prior to the

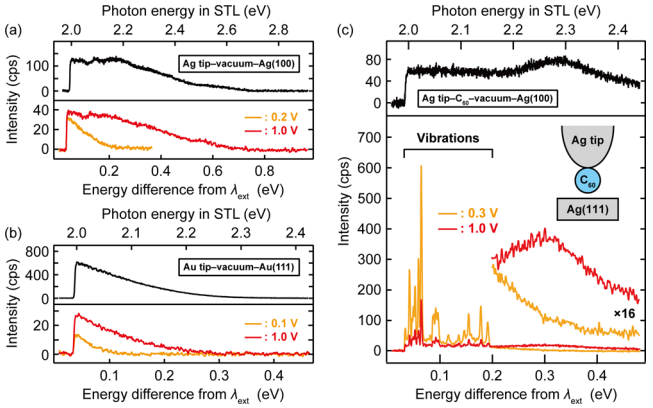

Figure 3. STL (top panel) and ILS spectra in the anti-Stokes regime (bottom panel) measured for different junctions. (a) Ag tip−vacuum−Ag(100) junction (STL: V_{bias} = 3 V, j_t = 9 nA, 10 K; ILS: λ_{ext} = 633 nm, P_{ext} = 0.34 mW μm^{-2}, j_t = 60 nA, 10 K), (b) Au tip−vacuum−Au(111) junction (STL: V_{bias} = 3 V, j_t = 5 nA, 10 K; ILS: λ_{ext} = 633 nm, P_{ext} = 0.34 mW μm^{-2}, I_t = 50 nA, 10 K), (c) Ag tip−single C_{60} molecule−Ag(111) junction (STL: V_{bias} = 3 V, j_t = 1 nA, 10 K; ILS: λ_{ext} = 633 nm, P_{ext} = 0.34 mW μm^{-2}, j_t = 60 nA, 10 K).

measurement.[59] For all cases the anti-Stokes continuum is observed and its onset coincides with the applied bias at a small V_{bias}, while the spectral shape becomes similar to that in STL at a large V_{bias}. For the Ag tip−single C_{60} molecule−vacuum−Ag(111) junction, the intense Raman peaks from molecular vibrations simultaneously appear (Figure 3c).

We propose the following model to rationalize the anti-Stokes continuum generation in the electrically biased plasmonic STM junction. Figure 4a illustrates the energy diagram of the STM junction. The ILS process involves the initial |i⟩, final |f⟩, and intermediate |e⟩ states. The horizontal thick lines represent one of the continuum states in the metals and their schematic wave functions are depicted by red curves.

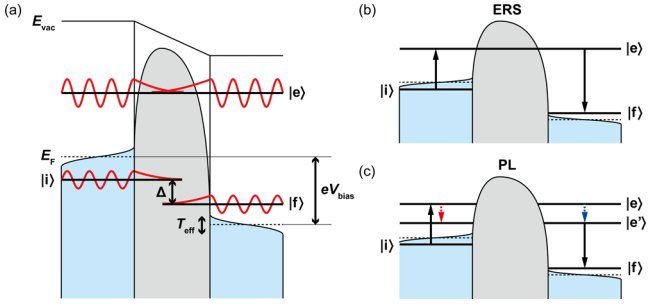

Figure 4. Schematic of the anti-Stokes scattering mechanism in an electrically biased plasmonic STM junction. (a) Energy diagram of the junction. The horizontal bold lines and the red curves represent one of the continuum states in the metal (tip/surface) and wave functions, respectively. |i⟩, |f⟩, and |e⟩ represent initial, final, and intermediate states, respectively. The gray shaded area represents the tunneling barrier. E_F: Fermi level; E_{vac}: vacuum level. (b) ERS occurs through coherent electron transfer from |i⟩ to |f⟩. (c) PL involves a population of the intermediate state(s) and subsequent dephasing/relaxation to |e′⟩ (another intermediate state) in the metal (tip/surface). The red and blue arrows represent the process involving dephasing/relaxation before and after electron transfer, respectively.

https://doi.org/10.1021/acsphotonics.1c00402
ACS Photonics 2021, 8, 2610−2617

The gray shaded area in Figure 4 represents the vacuum barrier. The dashed horizontal line represents the Fermi level of the tip/surface and the electron distribution is given by the effective temperature (T_{eff}) of the junction. The V_{bias}-dependence of the cutoff energy in Figure 2 suggests that the anti-Stokes scattering occurs through electron transfer across the junction during which the incident photon is inelastically scattered and gains the excess energy from the potential difference (V_{bias}). The barrier height is approximated by the work function of the metals (tip/surface), which is about 4.5 eV for Ag. The apparent barrier height for electron tunneling is not significantly affected by the tip−surface distance[60] unless the junction is close to the atomic point contact.[61] Therefore, the electron transfer should occur through the barrier (tunneling). The ERS and PL process should be at work simultaneously in ILS by plasmonic nanostructures. In ERS the electrons are coherently scattered from |i⟩ to |f⟩ and |e⟩ is not populated (Figure 4b). This process can happen efficiently or even be dominant when the LSPR of the junction is resonant with λ_{ext}. On the other hand, ERS becomes negligible if the LSPR is off resonant (or the LSPR is weak), instead PL becomes dominant. In PL the electron is first excited from |i⟩ to |e⟩, then followed by radiative damping from |e⟩ to |f⟩ to yield the anti-Stokes emission (Figure 4c). In this process the intermediate states are populated and dephasing (relaxation) of the excited state(s) is involved either before or after electron transfer across the junction.

The contribution from ERS or PL depends on spectral matching between the gap-mode plasmon and the excitation wavelength. We attempt to determine the relative contribution by examining how the local enhancement factor $g(\lambda)$ affects the anti-Stokes intensity while modifying the LSPR in the STM junction. By recording the STL and ILS spectra in parallel, we can characterize separately the gap-mode plasmon and the spectral response of ILS from the junction. The gap-mode plasmon was modified by applying a short voltage pulse in the junction that changes the tip apex structure. Near the excitation wavelength, the ERS intensity increases with $\sim g^4$ because the enhancement occurs in the incoming and outgoing electromagnetic field,[62,63] whereas the PL intensity is determined by the population of the excited state, thus, it is proportional to $\sim g^2$. However, in PL the nonradiative decay channel into metals also plays a role,[64] resulting in the net enhancement to be $\sim g^2\eta$, where $\eta \leq 1$ is the quantum yield of photoemission.[65,66] Therefore, the dependence of the ERS and PL cross section on the enhancement factor g should allow to clarify the major contribution. We evaluate a relative g for different tip conditions showing distinct LSPR properties. Figure 5a,b displays the STL and ILS spectra for λ_{ext} = 633 nm obtained under three different tip conditions. All the ILS spectra exhibit a similar spectral shape to the corresponding STL, but the relative intensity of ILS (I_{ILS}) near λ_{ext} differs from that of STL (I_{STL}). In STL, the enhancement acts only on the outgoing field, thus, the intensity follows $I_{STL} \propto g^2$. On the other hand, because the ERS intensity follows $I_{ERS} \propto g^4$, we can derive the intensity relation near λ_{ext} for the ERS process under two different tip conditions:

$$\frac{I'_{STL}}{I_{STL}} \approx \sqrt{\frac{I'_{ERS}}{I_{ERS}}} \quad (1)$$

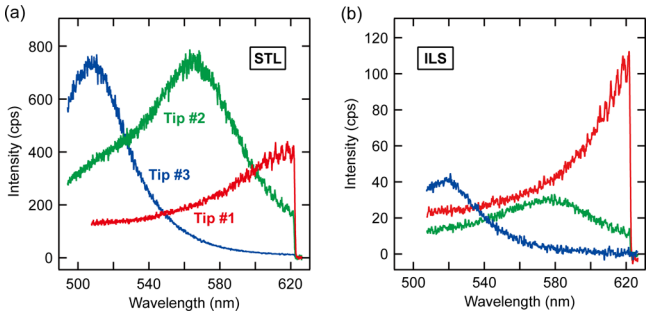

Figure 5. (a, b) STL and ILS spectra measured for three different tips, respectively. The measurement conditions are STL: V_{bias} = 3 V, j_t = 8 nA, 10 K; ILS: λ_{ext} = 633 nm, P_{ext} = 0.37 mW μm^{-2}, j_t = 60 nA, 10 K.

In Figure 5a,b, we find $\frac{I_{STL,tip\#2}}{I_{STL,tip\#1}} = 2.4(\pm 0.1)$ and $\sqrt{\frac{I_{ILS,tip\#2}}{I_{ILS,tip\#1}}} = \sqrt{8.6} = 2.9(\pm 0.1)$ at 620 nm, which is in good agreement with eq 1, indicating that ERS is the dominant process for tips #1 and #2. However, for tip #3 the I_{STL} near λ_{ext} is much smaller than that for tips #1 and #2, thus, $g_{tip\#1}(\lambda_{ext}) > g_{tip\#2}(\lambda_{ext}) \gg g_{tip\#3}(\lambda_{ext})$. In addition, I_{STL} and I_{ILS} of tip #3 does not satisfy the relation in eq 1, suggesting that the scattering mechanism is different, thus, PL should mainly contribute. A consistent relationship between I_{STL} and I_{ILS} was confirmed for various tip conditions (see Supporting Information, Figure S4). The above results indicate that ERS can be considerably enhanced in the presence of a strong LSPR around λ_{ext} in analogy to vibrational Raman scattering.[67,68] (The cross section of ERS ($<10^{-30}$) is as small as vibrational Raman scattering.[69,70])

It should be noted that the intensity and the spectral shape of STL significantly deviates from the ILS spectra through the PL process in some cases (Supporting Information, Figure S4). This may be explained by the fact that in the ILS measurement the LSPR excitation could occur in the tip base in addition to the very apex because the beam spot of ~3 μm is much larger than the apex (tens of nm), whereas the LSPR excitation in STL is strongly confined in the STM junction. Therefore, the latter case is more sensitive to the atomistic structure on the tip apex.

Typically, PL in noble metals involves interband transition from the *d*- to *sp*-band.[31,32] However, PL mediated by LSPR excitation can also occur through the intraband transition inside the *sp*-band because the momentum conservation could be satisfied by the large momentum uncertainty (Δk) of the confined plasmonic field.[19,37,71,72] According to recent low-temperature tip-enhanced Raman spectroscopy, the field confinement in the STM junction reaches even <1 nm,[53−55] thus, Δk will expand substantially across the Brillouin zone, allowing electronic transitions with a large momentum mismatch.

The number of electrons involved in the scattering process should be proportional to $\int_0^{eV_{bias}-\Delta} \rho(E)\, dE$, where Δ is the energy difference between |e⟩ and |f⟩ and $\rho(E)$ is the joint density of states. Because $\rho(E)$ is almost constant near the Fermi level, the intensity of the anti-Stokes continuum linearly depends on Δ. This relation is manifested in the spectral shape of the anti-Stokes continuum at a relatively small V_{bias}. As seen in Figures 2 and 3, the intensity linearly decreases as a function of the energy difference at V_{bias} < 0.3 V. It should be noted that the contribution to the anti-Stokes continuum from the

https://doi.org/10.1021/acsphotonics.1c00402
ACS Photonics 2021, 8, 2610−2617

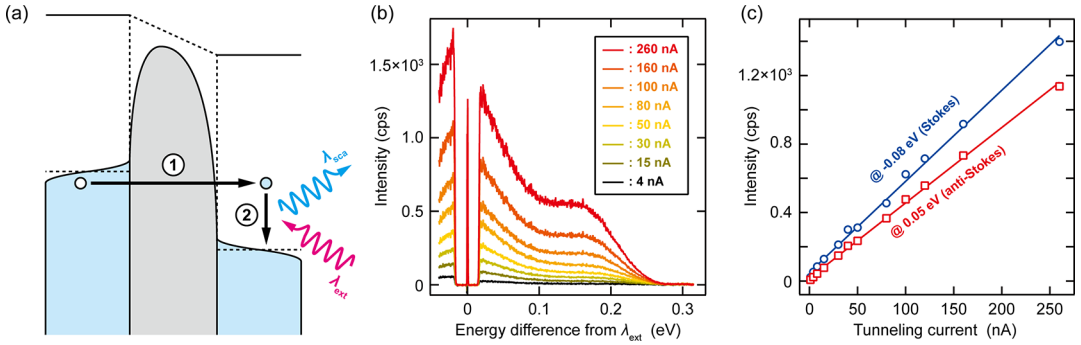

Figure 6. (a) Schematic of light scattering (step 2) after electron tunneling event (step 1) in the plasmonic STM junction (this mechanism is not operative). (b) j_t-dependence of the ILS spectra including the Stokes and anti-Stokes regime recorded for an Ag tip−vacuum−Ag(111) junction (λ_{ext} = 532 nm, P_{ext} = 0.25 mW μm^{-2}, V_{bias} = 0.5 V, 10 K). The j_t is indicated in the figure. (c) Stokes and anti-Stokes intensity at −0.08 and 0.05 eV in (b) as a function of the j_t.

thermally excited electrons (following the Fermi−Dirac distribution)[15] is negligible at 10 K of the measurement temperature. However, the junction could be optically heated. The cutoff energy of the anti-Stokes continuum appears to exceed the energy that is supplied by V_{bias}, which is obvious at V_{bias} < 0.3 V in Figure 2. This excess energy (the tail of the continuum) may be attributed to the elevated effective temperature of the electrons in the junction under irradiation,[73] whereby a part of the heated electrons above the Fermi level of the tip (surface) is scattered across the junction into the unoccupied states below the Fermi level of the surface (tip). At low V_{bias} (<0.3 V), the tip−surface distance becomes smaller and consequently optically induced heating will be more operative due to the stronger plasmonic field enhancement. In contrast, when the tip−surface distance is larger (at higher V_{bias}), the optical heating effect is not discernible. According to the mechanism in Figure 4, the ILS accompanied by electron transfer across the junction can also contribute to the Stokes scattering. This is indeed observed for the V_{bias}-dependence of the Stokes continuum (Supporting Information, Figure S5). Furthermore, the ILS process will lead to additional current because at least one electron is transferred upon one scattering event. Therefore, by integrating the intensity of the anti-Stokes continuum, we could estimate how many electrons are involved in the process, which is about ∼10^5 electrons per second at j_t of tens of nA. However, this is only a very small fraction (10^{-6}) of the total tunneling current (∼10^{11} electrons per second).

Finally, we examine another possible process to generate the anti-Stokes continuum. As illustrated in Figure 6a, the incident photons could interact with any excitation in the STM junction that occurs after V_{bias}-induced electron tunneling, for instance, hot-carrier generation in the tip or surface. In this case, the intensity of the anti-Stokes scattering should be proportional to the tunneling current (j_t), provided that the excitation is a one-electron process. Moreover, a larger j_t leads to larger field enhancement as the gap distance decreases. Figure 6b shows the intensity of the Stokes and anti-Stokes continuum as a function of j_t recorded for an Ag tip−vacuum−Ag(111) junction, revealing a linear dependence of both intensities. The intensity of the Stokes scattering (P_S) is governed by the field enhancement and the electronic structure of the junction, but it is not related to any excitations induced by the V_{bias}-induced tunneling electrons, thus, following $P_S \propto g^4$ for the ERS process. On the other hand, the anti-Stokes intensity follows $P_{AS} \propto j_t \times g^4$ if the process involved scattering with the excited states arising from the V_{bias}-induced tunneling electrons. Because P_S linearly depends on j_t in Figure 6c, the relation of $g^4 \propto j_t$ can be derived, thus, $P_{AS} \propto j_t^2$. However, this is clearly not the case in Figure 6c. Therefore, the above scenario can be discarded. Additionally, we observed a saturating behavior for the ILS intensity at very large j_t, that is, very small tip−surface distances (Supporting Information, Figure S6), which may result from attenuation of the plasmonic field through quantum effects, for example, nonlocal screening and electron tunneling.[74]

CONCLUSIONS

In conclusion, we showed that the anti-Stokes continuum occurs for electrically biased plasmonic STM junctions under narrow-band continuous-wave irradiation at the excitation wavelength below the interband transition of metals. The anti-Stokes continuum is commonly observed for various junctions at cryogenic temperature (∼10 K), including Ag tip−vacuum−Ag(111), Ag tip−vacuum−Ag(100), Au tip−vacuum−Au(111), and Ag tip−single C_{60} molecule−vacuum−Ag(111) junctions, indicating that it is a universal phenomenon. We showed that the incident photons gain the excess energy from the applied bias voltage and that two different mechanisms, namely ERS and PL mediated by electron transfer across the junction, are operative. A relative contribution from these two processes is governed by spectral matching of the gap-mode plasmon in the STM junction with the excitation wavelength. By recording ILS along with STM-induced luminescence, we demonstrated that the ERS process becomes dominant when the excitation wavelength matches the resonance of the gap-mode plasmon, whereas the PL process prevails under the off-resonance condition.

The present work provides an in-depth understanding of inelastic light scattering by plasmonic nanojunctions and demonstrates the nonthermal origin of the anti-Stokes continuum generation. The latter is intimately related to nanothermometry of plasmonic nanostructures. Although the electronic temperature can be estimated from the anti-Stokes continuum,[15] in electrically biased plasmonic nanojunctions, it should be carefully verified whether the spectral feature purely results from the local heating effect. In addition, recent experimental and theoretical studies have shown that the plasmonic properties in (sub)nanoscale cavities will be significantly affected by atomistic structures existing on the surface of metal nanostructures.[75−77] In this context, experiments in an atomically well-defined environment will be

https://doi.org/10.1021/acsphotonics.1c00402
ACS Photonics 2021, 8, 2610−2617

advantageous to elucidate the fundamental mechanisms of atomic-scale light−matter interactions.

■ ASSOCIATED CONTENT

Supporting Information

The Supporting Information is available free of charge at https://pubs.acs.org/doi/10.1021/acsphotonics.1c00402.

Incident laser power dependence of anti-Stokes continuum in an electrically biased STM junction, bias polarity dependence of the anti-Stokes continuum in an electrically biased STM junction, wavelength dependence of the anti-Stokes continuum in an electrically biased STM junction, tip dependence of the anti-Stokes continuum in an electrically biased STM junction, bias voltage dependence of the Stokes continuum in an electrically biased STM junction, and tunneling current dependence of the Stokes continuum in an electrically biased STM junction (PDF)

■ AUTHOR INFORMATION

Corresponding Author

Takashi Kumagai − *Department of Physical Chemistry, Fritz-Haber Institute of the Max-Planck Society, 14195 Berlin, Germany; Center for Mesoscopic Sciences, Institute for Molecular Science, Okazaki 444-8585, Japan;* orcid.org/0000-0001-7029-062X; Email: kuma@fhi-berlin.mpg.de, kuma@ims.ac.jp

Authors

Shuyi Liu − *Department of Physical Chemistry, Fritz-Haber Institute of the Max-Planck Society, 14195 Berlin, Germany*

Adnan Hammud − *Department of Inorganic Chemistry, Fritz-Haber Institute of the Max-Planck Society, 14195 Berlin, Germany*

Martin Wolf − *Department of Physical Chemistry, Fritz-Haber Institute of the Max-Planck Society, 14195 Berlin, Germany*

Complete contact information is available at: https://pubs.acs.org/10.1021/acsphotonics.1c00402

Funding

Open access funded by Max Planck Society.

Notes

The authors declare no competing financial interest.

■ ACKNOWLEDGMENTS

The authors thank Robert Schlögl for generous support for fabrication of FIB tips. T.K. acknowledges the support by JST-PRESTO (JPMJPR16S6).

■ REFERENCES

(1) Halas, N. J.; Lal, S.; Chang, W.-S.; Link, S.; Nordlander, P. Plasmons in Strongly Coupled Metallic Nanostructures. *Chem. Rev.* **2011**, *111* (6), 3913−3961.

(2) Hwang, Y.-N.; Jeong, D. H.; Shin, H. J.; Kim, D.; Jeoung, S. C.; Han, S. H.; Lee, J.-S.; Cho, G. Femtosecond Emission Studies on Gold Nanoparticles. *J. Phys. Chem. B* **2002**, *106* (31), 7581−7584.

(3) Varnavski, O. P.; Mohamed, M. B.; El-Sayed, M. A.; Goodson, T. Relative Enhancement of Ultrafast Emission in Gold Nanorods. *J. Phys. Chem. B* **2003**, *107* (14), 3101−3104.

(4) Dulkeith, E.; Niedereichholz, T.; Klar, T. A.; Feldmann, J.; von Plessen, G.; Gittins, D. I.; Mayya, K. S.; Caruso, F. Plasmon emission in photoexcited gold nanoparticles. *Phys. Rev. B: Condens. Matter Mater. Phys.* **2004**, *70* (20), 205424.

(5) Bouhelier, A.; Bachelot, R.; Lerondel, G.; Kostcheev, S.; Royer, P.; Wiederrecht, G. P. Surface Plasmon Characteristics of Tunable Photoluminescence in Single Gold Nanorods. *Phys. Rev. Lett.* **2005**, *95* (26), 267405.

(6) Varnavski, O. P.; Goodson, T., III; Mohamed, M. B.; El-Sayed, M. A. Femtosecond excitation dynamics in gold nanospheres and nanorods. *Phys. Rev. B: Condens. Matter Mater. Phys.* **2005**, *72* (23), 235405.

(7) Tcherniak, A.; Dominguez-Medina, S.; Chang, W.-S.; Swanglap, P.; Slaughter, L. S.; Landes, C. F.; Link, S. One-Photon Plasmon Luminescence and Its Application to Correlation Spectroscopy as a Probe for Rotational and Translational Dynamics of Gold Nanorods. *J. Phys. Chem. C* **2011**, *115* (32), 15938−15949.

(8) Fang, Y.; Chang, W.-S.; Willingham, B.; Swanglap, P.; Dominguez-Medina, S.; Link, S. Plasmon Emission Quantum Yield of Single Gold Nanorods as a Function of Aspect Ratio. *ACS Nano* **2012**, *6* (8), 7177−7184.

(9) Yorulmaz, M.; Khatua, S.; Zijlstra, P.; Gaiduk, A.; Orrit, M. Luminescence Quantum Yield of Single Gold Nanorods. *Nano Lett.* **2012**, *12* (8), 4385−4391.

(10) Neupane, B.; Zhao, L.; Wang, G. Up-Conversion Luminescence of Gold Nanospheres When Excited at Nonsurface Plasmon Resonance Wavelength by a Continuous Wave Laser. *Nano Lett.* **2013**, *13* (9), 4087−4092.

(11) Zhang, T.; Lu, G.; Shen, H.; Shi, K.; Jiang, Y.; Xu, D.; Gong, Q. Photoluminescence of a single complex plasmonic nanoparticle. *Sci. Rep.* **2015**, *4*, 3867.

(12) Huang, J.; Wang, W.; Murphy, C. J.; Cahill, D. G. Resonant secondary light emission from plasmonic Au nanostructures at high electron temperatures created by pulsed-laser excitation. *Proc. Natl. Acad. Sci. U. S. A.* **2014**, *111* (3), 906−911.

(13) Huang, D.; Byers, C. P.; Wang, L.-Y.; Hoggard, A.; Hoener, B.; Dominguez-Medina, S.; Chen, S.; Chang, W.-S.; Landes, C. F.; Link, S. Photoluminescence of a Plasmonic Molecule. *ACS Nano* **2015**, *9* (7), 7072−7079.

(14) He, Y.; Xia, K.; Lu, G.; Shen, H.; Cheng, Y.; Liu, Y.-C.; Shi, K.; Xiao, Y.-F.; Gong, Q. Surface enhanced anti-Stokes one-photon luminescence from single gold nanorods. *Nanoscale* **2015**, *7*, 577−582.

(15) Hugall, J. T.; Baumberg, J. J. Demonstrating Photoluminescence from Au is Electronic Inelastic Light Scattering of a Plasmonic Metal: The Origin of SERS Backgrounds. *Nano Lett.* **2015**, *15* (4), 2600−2604.

(16) Andersen, S. K. H.; Pors, A.; Bozhevolnyi, S. I. Gold Photoluminescence Wavelength and Polarization Engineering. *ACS Photonics* **2015**, *2* (3), 432−438.

(17) Haug, T.; Klemm, P.; Bange, S.; Lupton, J. M. Hot-Electron Intraband Luminescence from Single Hot Spots in Noble-Metal Nanoparticle Films. *Phys. Rev. Lett.* **2015**, *115* (6), No. 067403.

(18) Roloff, L.; Klemm, P.; Gronwald, I.; Huber, R.; Lupton, J. M.; Bange, S. Light Emission from Gold Nanoparticles under Ultrafast Near-Infrared Excitation: Thermal Radiation, Inelastic Light Scattering, or Multiphoton Luminescence? *Nano Lett.* **2017**, *17* (12), 7914−7919.

(19) Mertens, J.; Kleemann, M.-E.; Chikkaraddy, R.; Narang, P.; Baumberg, J. J. How Light Is Emitted by Plasmonic Metals. *Nano Lett.* **2017**, *17* (4), 2568−2574.

(20) Cai, Y.-Y.; Sung, E.; Zhang, R.; Tauzin, L. J.; Liu, J. G.; Ostovar, B.; Zhang, Y.; Chang, W.-S.; Nordlander, P.; Link, S. Anti-Stokes Emission from Hot Carriers in Gold Nanorods. *Nano Lett.* **2019**, *19* (2), 1067−1073.

(21) Otto, A. Raman scattering from adsorbates on silver. *Surf. Sci.* **1980**, *92* (1), 145−152.

(22) Birke, R. L.; Lombardi, J. R.; Gersten, J. I. Observation of a Continuum in Enhanced Raman Scattering from a Metal-Solution Interface. *Phys. Rev. Lett.* **1979**, *43* (1), 71−75.

(23) Tsang, J. C.; Kirtley, J. R.; Theis, T. N. Surface plasmon polariton contributions to strokes emission from molecular mono-

layers on periodic Ag surfaces. *Solid State Commun.* **1980**, *35* (9), 667−670.
(24) Pettinger, B.; Domke, K. F.; Zhang, D.; Picardi, G.; Schuster, R. Tip-enhanced Raman scattering: Influence of the tip-surface geometry on optical resonance and enhancement. *Surf. Sci.* **2009**, *603* (10−12), 1335−1341.
(25) Maruyama, Y.; Futamata, M. Inelastic scattering and emission correlated with enormous SERS of dye adsorbed on Ag nanoparticles. *Chem. Phys. Lett.* **2005**, *412* (1−3), 65−70.
(26) Michaels, A. M.; Jiang, J.; Brus, L. Ag Nanocrystal Junctions as the Site for Surface-Enhanced Raman Scattering of Single Rhodamine 6G Molecules. *J. Phys. Chem. B* **2000**, *104* (50), 11965−11971.
(27) Lin, K.-Q.; Yi, J.; Zhong, J.-H.; Hu, S.; Liu, B.-J.; Liu, J.-Y.; Zong, C.; Lei, Z.-C.; Wang, X.; Aizpurua, J.; Esteban, R.; Ren, B. Plasmonic photoluminescence for recovering native chemical information from surface-enhanced Raman scattering. *Nat. Commun.* **2017**, *8*, 14891.
(28) Otto, A.; Akemann, W.; Pucci, A. Normal Bands in Surface-Enhanced Raman Scattering (SERS) and Their Relation to the Electron-Hole Pair Excitation Background in SERS. *Isr. J. Chem.* **2006**, *46* (3), 307−315.
(29) Inagaki, M.; Isogai, T.; Motobayashi, K.; Lin, K.-Q.; Ren, B.; Ikeda, K. Electronic and vibrational surface-enhanced Raman scattering: from atomically defined Au(111) and (100) to roughened Au. *Chem. Sci.* **2020**, *11*, 9807−9817.
(30) Mukamel, S. *Principles of Nonlinear Optical Spectroscopy*; Oxford Universiy Press, 1995.
(31) Mooradian, A. Photoluminescence of Metals. *Phys. Rev. Lett.* **1969**, *22* (5), 185−187.
(32) Apell, P.; Monreal, R.; Lundqvist, S. Photoluminescence of noble metals. *Phys. Scr.* **1988**, *38* (2), 174−179.
(33) Otto, A.; Timper, J.; Billmann, J.; Kovacs, G.; Pockrand, I. Surface roughness induced electronic Raman scattering. *Surf. Sci.* **1980**, *92* (1), L55−L57.
(34) Dey, S.; Banik, M.; Hulkko, E.; Rodriguez, K.; Apkarian, V. A.; Galperin, M.; Nitzan, A. Observation and analysis of Fano-like lineshapes in the Raman spectra of molecules adsorbed at metal interfaces. *Phys. Rev. B: Condens. Matter Mater. Phys.* **2016**, *93* (3), No. 035411.
(35) Boyd, G. T.; Yu, Z. H.; Shen, Y. R. Photoinduced luminescence from the noble metals and its enhancement on roughened surfaces. *Phys. Rev. B: Condens. Matter Mater. Phys.* **1986**, *33* (12), 7923−7936.
(36) Mohamed, M. B.; Volkov, B.; Link, S.; El-Sayed, M. A. The 'lightning' gold nanorods: fluorescence enhancement of over a million compared to the gold metal. *Chem. Phys. Lett.* **2000**, *317* (6), 517−523.
(37) Beversluis, M. R.; Bouhelier, A.; Novotny, L. Continuum generation from single gold nanostructures through near-field mediated intraband transitions. *Phys. Rev. B: Condens. Matter Mater. Phys.* **2003**, *68* (11), 115433.
(38) Steiner, M.; Debus, C.; Failla, A. V.; Meixner, A. J. Plasmon-Enhanced Emission in Gold Nanoparticle Aggregates. *J. Phys. Chem. C* **2008**, *112* (8), 3103−3108.
(39) Shalaev, V. M.; Douketis, C.; Haslett, T.; Stuckless, T.; Moskovits, M. Two-photon electron emission from smooth and rough metal films in the threshold region. *Phys. Rev. B: Condens. Matter Mater. Phys.* **1996**, *53* (16), 11193−11206.
(40) Zurita-Sanchez, J. R.; Novotny, L. Multipolar interband absorption in a semiconductor quantum dot. I. Electric quadrupole enhancement. *J. Opt. Soc. Am. B* **2002**, *19* (6), 1355−1362.
(41) Carattino, A.; Keizer, V. I. P.; Schaaf, M. J. M.; Orrit, M. Background Suppression in Imaging Gold Nanorods through Detection of Anti-Stokes Emission. *Biophys. J.* **2016**, *111* (11), 2492−2499.
(42) Carattino, A.; Caldarola, M.; Orrit, M. Gold Nanoparticles as Absolute Nanothermometers. *Nano Lett.* **2018**, *18* (2), 874−880.
(43) Jones, S.; Andrén, D.; Karpinski, P.; Käll, M. Photothermal Heating of Plasmonic Nanoantennas: Influence on Trapped Particle Dynamics and Colloid Distribution. *ACS Photonics* **2018**, *5* (7), 2878−2887.
(44) Xie, X.; Cahill, D. G. Thermometry of plasmonic nanostructures by anti-Stokes electronic Raman scattering. *Appl. Phys. Lett.* **2016**, *109*, 183104.
(45) Marinica, D. C.; Zapata, M.; Nordlander, P.; Kazansky, A. K.; Echenique, P. M.; Aizpurua, J.; Borisov, A. G. Active quantum plasmonics. *Sci. Adv.* **2015**, *1* (11), No. e1501095.
(46) Mennemanteuil, M.-M.; Colas-des-Francs, G.; Buret, M.; Dasgupta, A.; Cuadrado, A.; Alda, J.; Bouhelier, A. Laser-induced thermoelectric effects in electrically biased nanoscale constrictions. *Nanophotonics* **2018**, *7* (12), 1917−1927.
(47) Ahmadivand, A.; Gerislioglu, B. Tunable plexciton dynamics in electrically biased nanojunctions. *J. Appl. Phys.* **2020**, *128*, No. 063101.
(48) Fung, E.-D.; Venkataraman, L. Too Cool for Blackbody Radiation: Overbias Photon Emission in Ambient STM Due to Multielectron Processes. *Nano Lett.* **2020**, *20* (12), 8912−8918.
(49) Rossel, F.; Pivetta, M.; Schneider, W.-D. Luminescence experiments on supported molecules with the scanning tunneling microscope. *Surf. Sci. Rep.* **2010**, *65* (5), 129−144.
(50) Zhang, C.; Chen, L.; Zhang, R.; Dong, Z. Scanning tunneling microscope based nanoscale optical imaging of molecules on surfaces. *Jpn. J. Appl. Phys.* **2015**, *54*, No. 08LA01.
(51) Berndt, R.; Gimzewski, J. K.; Johansson, P. Inelastic tunneling excitation of tip-induced plasmon modes on noble-metal surfaces. *Phys. Rev. Lett.* **1991**, *67* (21), 3796−3799.
(52) Kuhnke, K.; Große, C.; Merino, P.; Kern, K. Atomic-Scale Imaging and Spectroscopy of Electroluminescence at Molecular Interfaces. *Chem. Rev.* **2017**, *117* (7), 5174−5222.
(53) Lee, J.; Crampton, K. T.; Tallarida, N.; Apkarian, V. A. Visualizing vibrational normal modes of a single molecule with atomically confined light. *Nature* **2019**, *568*, 78−82.
(54) Zhang, Y.; Yang, B.; Ghafoor, A.; Zhang, Y.; Zhang, Y.-F.; Wang, R.-P.; Yang, J.-L.; Luo, Y.; Dong, Z.-C.; Hou, J. G. Visually Constructing the Chemical Structure of a Single Molecule by Scanning Raman Picoscopy. *Natl. Sci. Rev.* **2019**, *6*, 1169.
(55) Yang, B.; Chen, G.; Ghafoor, A.; Zhang, Y.; Zhang, Y.; Zhang, Y.; Luo, Y.; Yang, J.; Sandoghdar, V.; Aizpurua, J.; Dong, Z.; Hou, J. G. Sub-nanometre resolution in single-molecule photoluminescence imaging. *Nat. Photonics* **2020**, *14*, 693−699.
(56) Böckmann, H.; Liu, S.; Müller, M.; Hammud, A.; Wolf, M.; Kumagai, T. Near-Field Manipulation in a Scanning Tunneling Microscope Junction with Plasmonic Fabry-Pérot Tips. *Nano Lett.* **2019**, *19*, 3597−3602.
(57) Schull, G.; Néel, N.; Johansson, P.; Berndt, R. Electron-Plasmon and Electron-Electron Interactions at a Single Atom Contact. *Phys. Rev. Lett.* **2009**, *102* (5), No. 057401.
(58) Peters, P.-J.; Xu, F.; Kaasbjerg, K.; Rastelli, G.; Belzig, W.; Berndt, R. Quantum coherent multielectron processes in an atomic scale contact. *Phys. Rev. Lett.* **2017**, *119* (6), No. 066803.
(59) Schull, G.; Frederiksen, T.; Arnau, A.; Sanchez-Portal, D.; Berndt, R. Atomic-scale engineering of electrodes for single-molecule contacts. *Nat. Nanotechnol.* **2011**, *6*, 23−27.
(60) Olesen, L.; Brandbyge, M.; Sørensen, M. R.; Jacobsen, K. W.; Lægsgaard, E.; Stensgaard, I.; Besenbacher, F. Apparent Barrier Height in Scanning Tunneling Microscopy Revisited. *Phys. Rev. Lett.* **1996**, *76* (9), 1485−1488.
(61) Kröger, J.; Jensen, H.; Berndt, R. Conductance of tip−surface and tip−atom junctions on Au(111) explored by a scanning tunnelling microscope. *New J. Phys.* **2007**, *9*, 153.
(62) Le Ru, E. C.; Etchegoin, P. G. Rigorous justification of the $|E|^4$ enhancement factor in surface enhanced Raman spectroscopy. *Chem. Phys. Lett.* **2006**, *423*, 63−66.
(63) Ding, S.-Y.; Yi, J.; Li, J.-F.; Ren, B.; Wu, D.-Y.; Panneerselvam, R.; Tian, Z.-Q. Nanostructure-based plasmon-enhanced Raman spectroscopy for surface analysis of materials Nat. *Rev. Mater.* **2016**, *1*, 16021.

https://doi.org/10.1021/acsphotonics.1c00402
ACS Photonics 2021, 8, 2610−2617

(64) Anger, P.; Bharadwaj, P.; Novotny, L. Enhancement and quenching of single-molecule fluorescence. *Phys. Rev. Lett.* **2006**, *96* (11), 113002.
(65) Farahani, J. N.; Pohl, D. W.; Eisler, H.-J.; Hecht, B. Single quantum dot coupled to a scanning optical antenna: A tunable superemitter. *Phys. Rev. Lett.* **2005**, *95* (1), No. 017402.
(66) Thomas, M.; Greffet, J.-J.; Carminati, R.; Arias-Gonzalez, J. R. Single-molecule spontaneous emission close to absorbing nanostructures. *Appl. Phys. Lett.* **2004**, *85* (17), 3863−3865.
(67) Zhang, R.; Zhang, Y.; Dong, Z. C.; Jiang, S.; Zhang, C.; Chen, L. G.; Zhang, L.; Liao, Y.; Aizpurua, J.; Luo, Y.; Yang, J. L.; Hou, J. G. Chemical mapping of a single molecule by plasmon-enhanced Raman scattering. *Nature* **2013**, *498*, 82−86.
(68) Liu, S.; Müller, M.; Sun, Y.; Hamada, I.; Hammud, A.; Wolf, M.; Kumagai, T. Resolving the Correlation between Tip-Enhanced Resonance Raman Scattering and Local Electronic States with 1 nm Resolution. *Nano Lett.* **2019**, *19* (8), 5725−5731.
(69) Koningstein, J. A.; Mortensen, O. S. Electronic Raman Spectra. III. Absolute Cross Sections for Electronic Raman and Rayleigh Scattering. *Phys. Rev.* **1968**, *168* (1), 75−78.
(70) Koningstein, J. A.; Ng, T. Electronic Raman effect of dysprosium ion. *Solid State Commun.* **1969**, *7* (2), 351−354.
(71) Noda, M.; Iida, K.; Yamaguchi, M.; Yatsui, T.; Nobusada, K. Direct Wave-Vector Excitation in an Indirect-Band-Gap Semiconductor of Silicon with an Optical Near-field. *Phys. Rev. Appl.* **2019**, *11* (4), No. 044053.
(72) Yatsui, T.; Okada, S.; Takemori, T.; Sato, T.; Saichi, K.; Ogamoto, T.; Chiashi, S.; Maruyama, S.; Noda, M.; Yabana, K.; Iida, K.; Nobusada, N. Enhanced photo-sensitivity in a Si photodetector using a near-field assisted excitation. *Commun. Phys.* **2019**, *2*, 62.
(73) Ward, D. R.; Corley, D. A.; Tour, J. M.; Natelson, D. Vibrational and electronic heating in nanoscale junctions. *Nat. Nanotechnol.* **2011**, *6*, 33−38.
(74) Zhu, W.; Esteban, R.; Borisov, A. G.; Baumberg, J. J.; Nordlander, P.; Lezec, H. J.; Aizpurua, J.; Crozier, K. B. Quantum mechanical effects in plasmonic structures with subnanometre gaps. *Nat. Commun.* **2016**, *7*, 11495.
(75) Benz, F.; Schmidt, M. K.; Dreismann, A.; Chikkaraddy, R.; Zhang, Y.; Demetriadou, A.; Carnegie, C.; Ohadi, H.; de Nijs, B.; Esteban, R.; Aizpurua, J.; Baumberg, J. J. Single-molecule optomechanics in "picocavities. *Science* **2016**, *354*, 726−729.
(76) Zhang, P.; Feist, J.; Rubio, A.; García-González, P.; García-Vidal, F. J. Ab initio nanoplasmonics: The impact of atomic structure. *Phys. Rev. B: Condens. Matter Mater. Phys.* **2014**, *90* (16), 161407.
(77) Urbieta, M.; Barbry, M.; Zhang, Y.; Koval, P.; Sánchez-Portal, D.; Zabala, N.; Aizpurua, J. Atomic-Scale Lightning Rod Effect in Plasmonic Picocavities: A Classical View to a Quantum Effect. *ACS Nano* **2018**, *12* (1), 585−595.

https://doi.org/10.1021/acsphotonics.1c00402
ACS Photonics 2021, 8, 2610−2617